

Combined Gamma-Ray/Neutron Imaging System for Detecting Nuclear Material

Lakshmi Soundara-Pandian¹, Jarek Glodo, James F. Christian, Robert Vinci, Andrey Gueorguiev, Chad Whitney, Erik B. Johnson, Kanai S. Shah, Michael R. Squillante

Radiation Monitoring Devices, Inc. 44 Hunt Street, Watertown, MA 02472

ABSTRACT

Intercepting and identifying potentially dangerous radioactive materials and nuclear weapons is a high priority issue both for homeland security and for protecting our warfighters. In addition to locating radioactive sources, imaging can improve signal-to-noise ratio and provide higher sensitivity than discrete detectors. This can also reduce the frequency of false alarms since some legitimate sources and NORM can be readily identified as not being threats from the image. Thus, better nuclear imaging systems with both gamma-ray and neutron imaging capabilities would be of significant value for improved detection of such materials. To address this critical problem, RMD is investigating the design and construction of a portable gamma-ray/neutron imaging system based on RMD's successful RadCamTM instrument.

The instrument, which is based on the new generation of scintillator materials that have the capability to discriminate gamma rays from neutrons, will simultaneously image gamma rays and neutrons. Detecting and imaging neutrons provides the ability to detect sources that are heavily shielded for gamma rays. Since few materials emit neutrons, the presence of neutrons in the image is a strong indicator of the presence of fissile material. The system would also be useful for active interrogation. This paper will discuss camera design and examine the trade-offs needed to optimize both the gamma ray and neutrons imaging systems and present measured gamma and neutron images.

INTRODUCTION

Effective monitoring of special nuclear materials (SNM) benefits from the detection of both gamma and neutron radiation. Since neutrons are not generated from any naturally occurring radioactive decay and the neutron background is reasonably constant and low, the detection of neutrons can provide a sensitive approach to indicate the presence of spontaneous fission of isotopes (plutonium and californium) and induced fissions as in uranium. Imaging techniques provide additional advantage of increased signal-to-noise ratio above simple detection and provide source localization. A number of techniques for imaging gamma-rays and neutrons have been developed, such as pin hole cameras [1], coded-aperture configurations [2-4], and telescopic configurations for neutrons [5] and Compton imaging [6,7], as well as multi-mode approaches that combine different techniques [8,9]. Coded-aperture configurations are relatively simple and

¹ Manuscript received on June 7, 2013. The corresponding author L. Soundara-Pandian is with Radiation Monitoring Devices, Inc., Watertown, MA 02472.(email: lspondian@rmdinc.com)

provide good sensitivity and resolution, spatial and energy, especially for low energy gamma-ray imaging.

To develop a camera with both gamma-ray and neutron imaging capability, RMD is investigating the design and construction of a portable gamma-ray/neutron imaging system based on RMD's commercial RadCam™ instrument, which is a coded-aperture configuration. In this paper we report on the first generation CLYC-RadCam prototype developed at RMD.

RADCAM

RadCam™ [10] is a gamma-ray imaging system developed by RMD for tracking radiation contamination and distribution. A square, 2"x.2" CsI:Na scintillator coupled to a position sensitive photomultiplier (PSPMT) detects the gamma-rays and provides the image plane for the MURA (modified uniformly redundant array) coded aperture, or an interchangeable pin-hole aperture. Detected signals are decoded to produce radiation image that is overlaid on an optical image from a video camera. *Figure 1* (left) shows a photograph of the RadCam system (light version with limited shielding) mounted on a robot. The system was tested at the nuclear reactor of University of Michigan. The system detects gamma radiation and creates a heat map, which is overlapped on a photograph of the investigated area. The software has the capability of gating on particular section of the map to pull energy spectra and investigate type of the source. It is also possible to gate the system according to the energy and create heat maps corresponding to selected energy slices (right) shows an image of the filtrations system and waste storage drums recorded at the nuclear reactor service room (University of Michigan). The intensity map of the radiation distribution is shown superimposed on a photograph



Figure 1 (Left) Remote RadCam system tested at University of Michigan nuclear reactor. (Right) The RadCam image recorded at the University of Michigan nuclear reactor service room of the filtrations system and waste storage drums. The image shows the location of radioactive material in the drums.

Table 1 Current RadCam™ Specifications

Property	Value
Field of View	10 m ² at 10 m
Energy Resolution	23% at 662 keV
Angular Resolution	2.3° to 14° at 10 m
Acquisition Time	40 s for 1 mCi at 5 m
Energy Sensitivity for Gammas	< 30 keV to > 1.5 MeV
Lower Detection Limit	100 nCi/cm ²
Portability	High – Weight 100 lbs or less
Imager Mechanical Complexity	Low
Operator control distance from imager	Variable 0-10 m

of investigated area. The image shows the location of radioactive material in the drums. The specifications of the current RadCam system are listed in *Table 1*.

CLYC – RADCAM PROTOTYPE

The goal of the effort is to incorporate CLYC in the current RadCam system, adding neutron detection capabilities to the system and investigate capabilities for neutron imaging. The system will find its applications in monitoring and tracking of radiation contamination. In the first generation CLYC-RadCam system (see *Figure 2*) the 2-inch x 2-inch square CsI:Na crystal was replaced with a 2-inch diameter circular CLYC crystal, the 38 x 38 MURA coded-aperture tungsten mask was replaced with a 7 x 7 MURA coded-aperture tungsten and cadmium mask, and cadmium shielding was added. In the sections below, we describe the CLYC crystal, the calibration and characterization of the crystal, and the mask used in the CLYC RadCam.

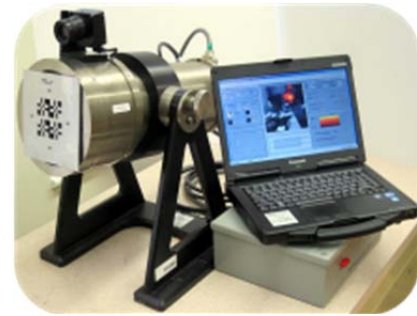


Figure 2 Picture of the CLYC-RadCam prototype

A. CLYC

CLYC [11, 12] has been under development at RMD for dual gamma ray and neutron detection in hand-held, pagers and other radiation detectors. The material is capable of providing good gamma ray spectroscopy with the best energy resolution of better than 4% at 662 keV. This is better than the “typical” ~7.5% at 662 keV energy resolution of CsI:Na, scintillation material. Our initial results show that substituting CsI:Na with CLYC on the PSPMT improves the energy resolution. *Table 2* lists a summary of the scintillation properties of both crystals.

Table 2 Scintillation properties of CLYC:Ce and CsI:Na

Property	CLYC:Ce	CsI:Na
Density, g/cc	3.3	4.5
Emission, nm	380	420
Decay time, ns	60, 900	630
Light yield, ph/MeV	20,000	41,000
Best resolution @662keV, % ^(*)	3.6	7
Neutron detection	Yes	No
Hygroscopic	Yes	Yes

(*) Measured on a R6233-100 PMT.



Figure 3 Picture of the 2-inch diameter, 5mm thick CLYC crystal packaged in an airtight package.

CLYC’s capabilities go beyond good energy resolution. Due to the presence of ⁶Li, the material can also detect thermal neutrons. The detection efficiency is as good as He-3 detectors. The separation between gamma ray and neutron signals can be achieved either using pulse height or

shape discrimination [11]. Recently, it has been shown that CLYC can also detect fast neutrons either due to ${}^6\text{Li}$ or ${}^{35}\text{Cl}$ interactions [13, 14, 15 and 16].

A picture of the 2''-diameter CLYC crystal is shown in *Figure 3*. In the CLYC RadCam camera, the crystal is coupled to a Hamamatsu R2486 Position-sensitive (PS) PMT. We calibrate the detector unit using a “look-up” table to correlate the real position to the measured position, as well as excluding the corner locations. The characterization measurements include evaluating the energy resolution performance and the imaging performance of the prototype.

B. Calibration

The purpose of the calibration is to generate a look-up table that correlates the real position to the measured position based on the charge division of the detector. The RadCam imaging system uses a position sensitive PMT to derive the XY spatial location of photons from the CLYC crystal impacting the photocathode face. The photoelectrons emitted from the face are accelerated through multiple dynode stages and impact a 38 x 38 mesh grid. The X wires and Y wires are connected to a voltage divider network. By measuring the differential signal from the ends of each voltage divider network a spatial position may be obtained. There are several sources of nonlinearities that can affect the accurate determination of the XY position. These include:

- Positioning of the scintillator crystal with respect to the PMT face
- Boundary effects of the PMT response at the edges of the XY grid
- Boundary effects of the PMT and CLYC Crystal

To account for these effects a calibration procedure was created to measure the CLYC-RadCam system response at each point of the XY mesh intersections.

The X-Y calibration setup used is shown *Figure 4* on left. In the case of the circular CLYC crystal, the calibration process reveals distortions in the corners of the range map. Hence, the process was modified to “over scan” the crystal area. In addition, we used a circular exclusion mask (defined by the circular crystal geometry) that excludes regions of the scan data to eliminate non-relevant data generated during the raw scanning process. This method used a 38x38 binary coded mask file to select the region of interest and exclude the rest. Calibration map generated for the circular CLYC crystal with square and circular masks are shown in *Figure 4* on right.

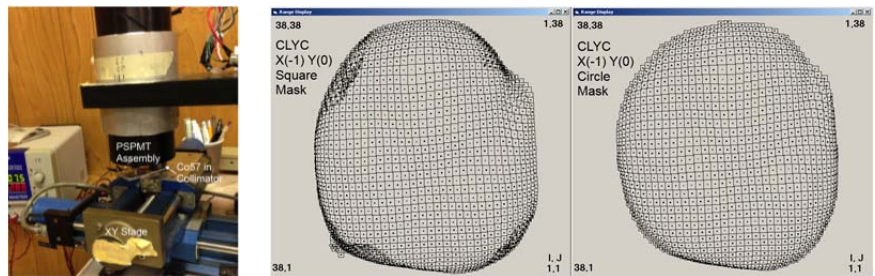


Figure 4 (Left) Calibration setup (Right) Range map for the circular CLYC crystal with a square look up grid and after the application of the exclusion mask

C. Energy Spectra and Pulse Shape Discrimination

Energy spectra obtained with the CLYC crystal coupled to the PSPMT are shown in *Figure 5* on the left. We obtain a resolution of $\sim 14\%$ at 662keV and 13% for thermal neutrons using standard NIM electronics consisting of preamplifier, spectroscopic amplifier and a MCA. For PSD measurements a CAEN DT 5720 digitizer was used. The pulse-shape discrimination [17] is obtained by taking ratio of two different time integration windows for the gamma and neutron waveforms. The PSD scatter plot obtained with the sum of four signals is shown on right in *Figure 5*. Neutrons and gamma rays are well separated. Therefore, it is possible to do pulse shape discrimination in the CLYC-RadCam prototype.

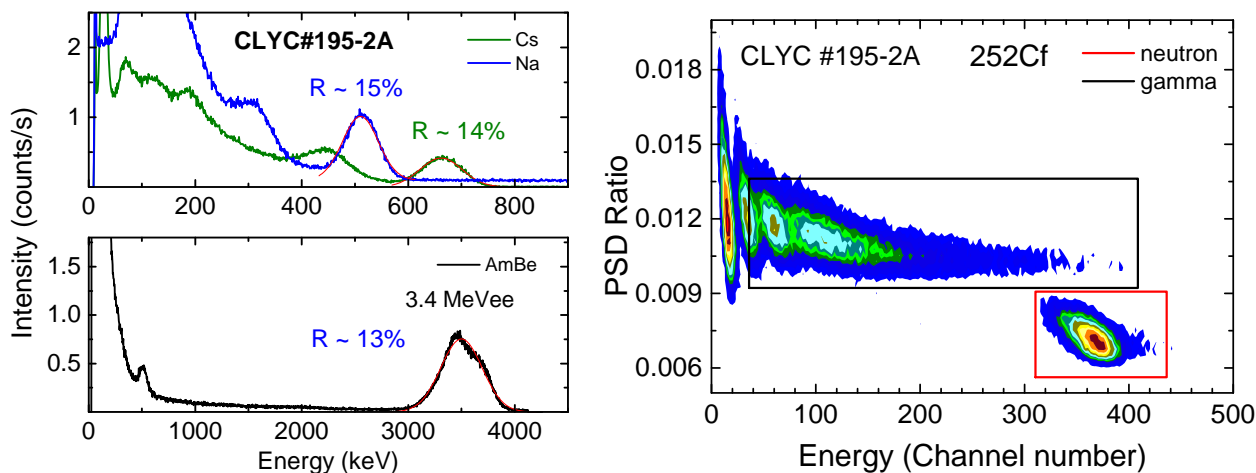


Figure 5 (Left) Gamma and Neutron energy spectra measured with the 2-inch diameter, 5mm thick CLYC crystal coupled to the RadCam PSPMT. (Right) PSD scatter plot obtained with ^{252}Cf source. Neutrons are well separated from the gamma-rays.

D. Coded-aperture Mask

Imaging characterization was performed using a 7x7 Cadmium and Tungsten MURA mask. The mask consists of 5mm-thick polymer with tungsten powder, with a density of approximately 13 g/cc in an 8-mm thick lead holder with a square hole. In addition, two 2-mm thick Cd plates with the same 7x7 MURA pattern are connected to the front. Photographs of the mask are shown in *Figure 6*; on left is the front side of the mask, which is the cadmium coded aperture for neutrons and shown on right is the back side which is tungsten coded aperture for gamma rays. Since original RadCam mask is 38x38 a 7x7 pattern file (G_2R_7x7.dat) is constructed to accommodate the 38x38 format in the RadCam software.

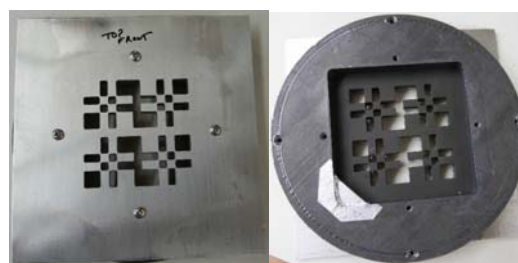


Figure 6 Double coded aperture (Left) Front side - Cadmium coded aperture (Right) Back side – Tungsten coded aperture.

IMAGING CHARACTERIZATION

The double coded aperture was used for imaging to reject background that may arise from room return. A setup of the imaging system is shown in *Figure 7*. A $39\mu\text{Ci } ^{252}\text{Cf}$ source was placed 2.5 feet away from the face of the imaging system. Both video and nuclear images were recorded for different source

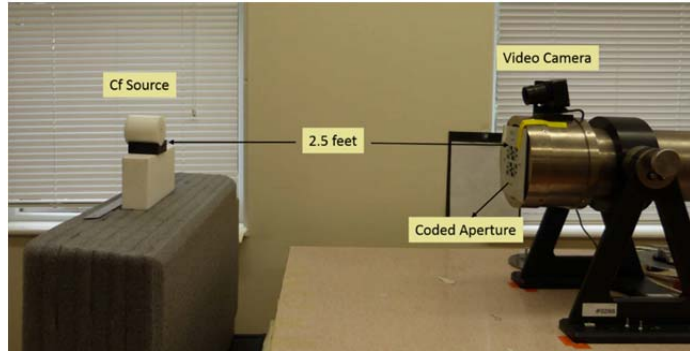


Figure 7 Picture of the gamma neutron imaging system.

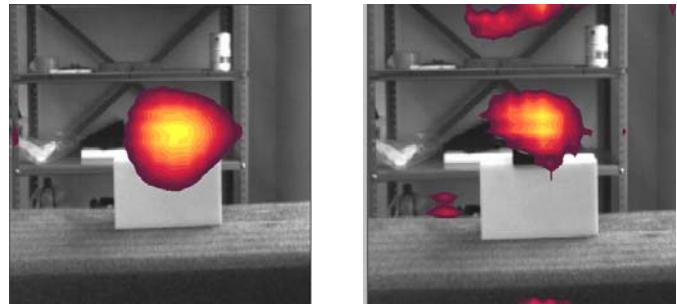
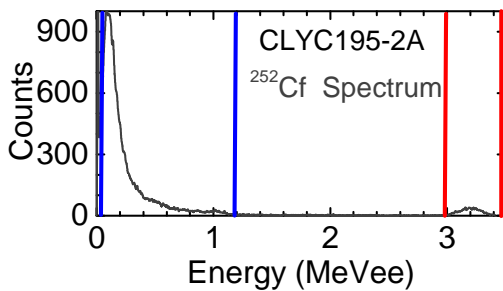


Figure 9 (Left) Energy spectrum obtained with the ^{252}Cf source placed at center. (Middle) Image gated on gamma rays (0 to 1 MeV - region enclosed between blue lines) (Right) Image gated on thermal neutrons (3 to 3.5 MeVee – region enclosed between red lines).

positions. Energy spectrum obtained with the ^{252}Cf source placed at center is shown in *Figure 9* on left. The region enclosed between the blue vertical lines shows the gamma gate from 0 to 1.1 MeV and the region between red lines shows the neutron gate from 3 to 3.5 MeVee. Images obtained with gamma and neutron gates with source at center are shown in the middle and right panels in *Figure 9*. Images obtained with source moved 5 inches right and left are shown in *Figure 8*. These images clearly demonstrate that we can image neutrons using our prototype system. We recorded approximately 1500 thermal neutron events in 2 hours.

To confirm the identity of the neutron features in the images, a neutron absorber was placed in front of the camera and data was collected for the same amount of time. A 4-mm-thick Cadmium thick sheet was used as the absorber. Image obtained with both neutrons and gamma-rays (no energy gate) is shown in *Figure 10* on left. In this image we see a

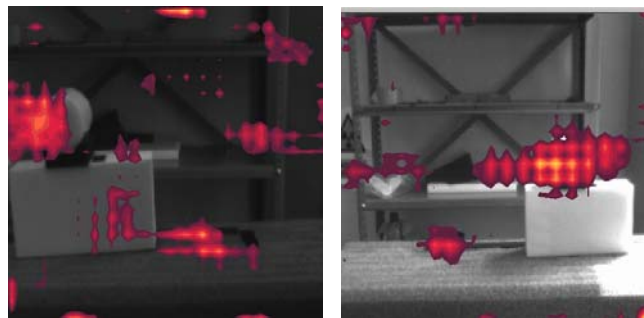


Figure 8 Neutron images obtained with source (left) moved left (right) moved right.

clear image from gamma-rays emitted from the ^{252}Cf source. When gated on 3 to 3.5 MeV neutrons gamma image disappears and we see a small neutron background, which is shown in image on right in *Figure 10*.

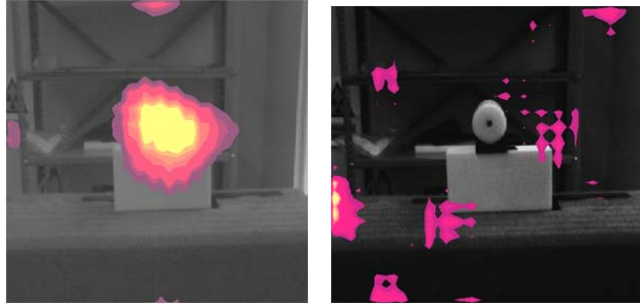


Figure 10 Images acquired with neutrons blocked. A 4mm thick Cadmium sheet was placed in front of the camera (Left) Gamma Image (Right) Image gated on neutrons.

EXTENDING CAPABILITIES

The second generation CLYC-RadCam will implement pulse-shape discrimination. In addition, we are looking at options for using a different photo multiplier tube, which provides a modular format for the detector plane. The H10966A, 2inch x 2inch square multi-anode PMT (MAPMT) seems to be a good choice to replace the current PSPMT. The square tube has a super

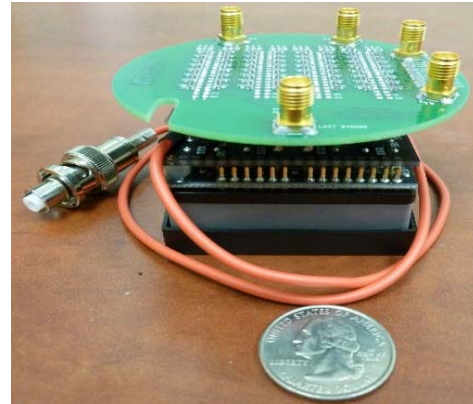
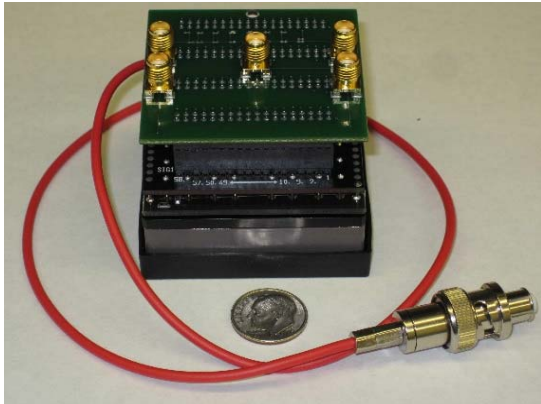


Figure 11 Read out boards for the H10966A multi-anode PMT (Left) Simple resistive board connected to the PMT (Right) Anode gain compensating readout board custom made for this PMT by Vertilon Corporation.

bi-alkali photo cathode, hence we expect improved performance compared to the bi-alkali PSPMT. On the other hand, the disadvantage of MAPMT is the anode gain non-uniformity. MAPMT provides 64 outputs, which need to be read.

To evaluate MAPMT, two different readout boards were made. The first board is a simple resistive readout board, which uses chain of resistors to reduce the 64 outputs to 4 outputs. Anger logic is used to reconstruct the position from the 4 signals. This board was made in house at RMD and a picture of this board mounted on the PMT is shown in *Figure 11* on left. Another readout board, which would compensate for anode gains, was obtained from the Vertilon Corporation [18]. This board was custom made with resistor values mapped to the gain variations provided by Hamamatsu [19]. A picture of this board is shown on right in *Figure 11*. Our initial evaluation of both boards started with testing a $0.7 \times 0.7 \times 1 \text{ in}^3$ CLYC crystal coupled to MAPMT. Energy

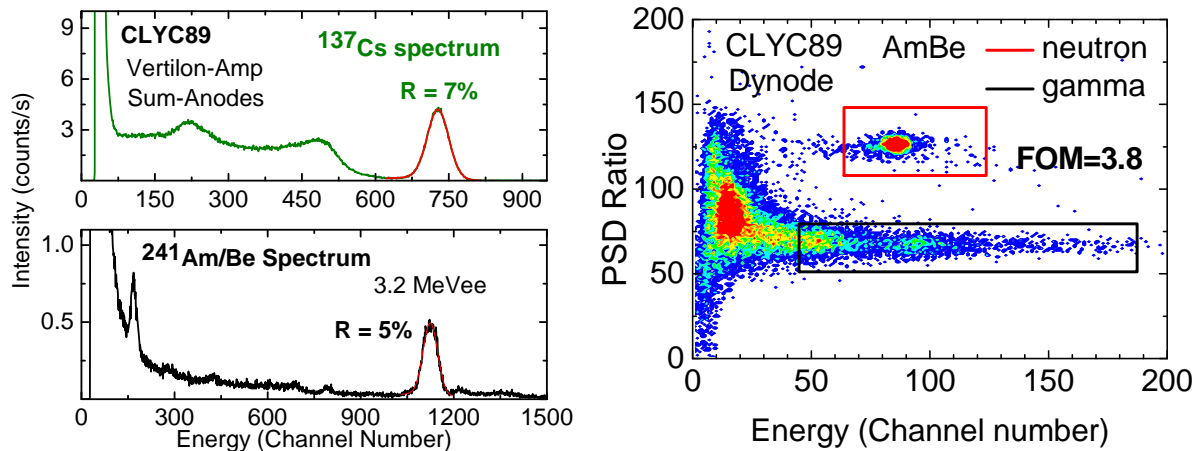


Figure 12 (Left) ^{137}Cs energy spectrum measured with CLYC 89 coupled to the square PMT. Simple resistive readout was used. (Right) PSD scatter plot measured using the last dynode output shows excellent separation.

spectra obtained with the gain compensating readout board with standard NIM electronics are shown in Figure 12 on left. We obtain a resolution of 7% at 662 keV and 5% at 3.2 MeVee thermal neutrons. However, for larger crystals the anode gain variations contribute to a worse resolution. Both readout boards were also tested for pulse shape discrimination. The last dynode output (DY8) was digitized using a CAEN DT5720 digitizer and 20K waveforms were recorded and analyzed offline. The PSD scatter plot obtained is shown on right in Figure 12. Neutrons are well separated from the gamma-rays and the figure of merit [17] obtained is 3.8.

SUMMARY

The CLYC-RadCam prototype has been demonstrated for its performance as a gamma-neutron imaging instrument. An energy resolution of 14% has been achieved at 662keV with a 2-inch diameter CLYC crystal coupled to the PSPMT used in the current RadCam, compared to 23% with CsI:Na. Gamma and neutron imaging have been achieved using a double coded aperture, which is a combination of cadmium and tungsten. In addition, pulse shape discrimination seems possible with the CLYC crystal coupled to the PSPMT. These results are very encouraging and the achievement of neutron imaging with Cd coded aperture is a very important step in making a portable gamma-neutron imaging instrument. The H10966A square MAPMT is being considered as a replacement in the next generation device. This PMT is being evaluated with two different readout boards. Future work will involve improving the energy resolution for large crystals. To summarize, this work has successfully demonstrated neutron imaging capabilities with the initial CLYC-RadCam prototype.

ACKNOWLEDGEMENTS

This work has been supported by the Defense Threat Reduction Agency, under competitively awarded contract/HDTRA1-12-C-0045. This support does not constitute an express or implied endorsement on the part of the Government. DISTRIBUTION A. Approved for public release: distribution unlimited.

REFERENCES

- [1] DiFilippo, F.P., *Design and performance of a multi-pinhole collimation device for small animal imaging with clinical SPECT and SPECT-CT scanners*. Phys. Med. Biol., 2008. **53**(15): p. 4185-4201.
- [2] Fenimore, E.E. and T.M. Cannon, *Coded aperture imaging with uniformly redundant arrays*. Appl. Opt., 1978. **17**: p. 337-347.
- [3] Ziock, K.P.C., W.W.; Fabris, L.; Lanza, R.C.; Gallagher, S.; Horn, B.K.P.; Madden, N.W., *Large Area Imaging Detector for Long-Range, Passive Detection of Fissile Material*. IEEE Trans. Nucl. Sci., 2004. **51**(5): p. 2238-2244.
- [4] Kowash, B.R., D.K. Wehe, and N.O. Boyce. *Extended source imaging using a single rotating modulation collimator*. in *IEEE Nucl. Sci. Symp. Conf. Record*.
- [5] Bravar, U., et al., *FNIT: the Fast Neutron Imaging Telescope for SNM Detection*. Proc. SPIE - Int. Soc. Opt. Eng. (USA), 2006. **6213**: p. 62130G1-9.
- [6] Kurfess, J.D., et al. *Considerations for the Next Compton Telescope Mission*. 1999. Portsmouth, New Hampshire.
- [7] Philips, B.F., et al., *Performance of a Compton Telescope using Position-Sensitive Germanium Detectors*. IEEE Trans. Nucl. Sci., 1996. **43**(3): p. 1472.
- [8] Smith, L.E., et al., *Design and Modeling of the Hybrid Portable Gamma Camera System*. IEEE Trans. Nucl. Sci., 1998. **43**(3): p. 963.
- [9] Christian, J.F., et al., *Nuclear material detection techniques*. Optics and Photonics in Global Homeland Security IV, 2008. **6945**.
- [10] M. Woodring, D. Beddingfield, D. Souza, G. Entine, M. Squillante, J. Christian, A. Kogan, "Advanced multi-dimensional imaging of gamma-ray radiation," Nuclear Inst. and Methods in Phys. Res. A., vol. 505, pp. 415-419, 2003.
- [11] J. Glodo, W. M. Higgins, E. V. D. van Loef, K. Shah, "Scintillation properties of 1 inch Cs₂LiYCl₆:Ce crystals," IEEE Trans. Nucl. Sci. vol. 55, pp. 1206-1209, June 2008.
- [12] Glodo, J., Higgins, W. M., Van Loef, E. V. D., Shah, K. S., "Cs₂LiYCl₆:Ce scintillator for nuclear monitoring applications," IEEE Trans. Nucl. Sci. vol. 56, no. 3, pp. 1257-1261, 2009.
- [13] T Achtzehn, H R Andrews, E T H Clifford, H Ing, V D Kovaltchouk, A Voeyodskiy, *Fast neutron spectroscopy using neutron-induced charged particle reactions*, Application number: 13/096,228, Publication number: US 2011/0266451 A1, Filing date: Apr 28, 2011.
- [14] D'Olympia, N.; Chowdhury, P.; Guess, C. J.; Harrington, T.; Jackson, E. G.; Lakshmi, S.; Lister, C. J.; Glodo, J.; Hawrami, R.; Shah, K.; Shirwadkar, U. "Optimizing Cs₂LiYCl₆ for fast neutron spectroscopy" Nuclear Instruments and Methods in Physics Research A, Volume 694, pp. 140-146, 2012
- [15] J. Glodo, U. Shirwadkar, R. Hawrami, T. Achtzehn, H. R. Andrews, E. T. H. Clifford, H. Ing, V. D. Kovaltchouk, M. B. Smith, and K. S. Shah, *Fast neutron detection with Cs₂LiYCl₆*, IEEE Trans. Nucl. Sci. vol. 60, No.2, pp. 864-870, April 2013
- [16] Martin B. Smith, Tobias Achtzehn, Hugh R. Andrews, Edward T. H. Clifford, Harry Ing and Vitali D. Kovaltchouk, *Fast neutron spectroscopy using Cs₂LiYCl₆:Ce(CLYC) scintillator*, IEEE Trans. Nucl. Sci. vol. 60, No.2, pp. 855-859, April 2013.

- [17] J. Glodo, R. Hawrami, E. V. D. Van Loef, U. Shirwadkar, and K. S. Shah, “*Pulse Shape Discrimination with Selected Elpasolite Crystals,*” IEEE Trans. Nucl. Sci. vol. 59(2), pp.2328-2333 (2012).
- [18] <http://www.vertilon.com/>
- [19] V. Popov, S. Majewski, B.L.Welch, *A novel readout concept for multianode photomultiplier tubes with pad matrix anode layout,* Nucl. Instr. Meth. Phys. Res. A, Vol 567, p.319, 2006